Fermilab

FERMILAB-Pub-01/390-E January 2002

CDF/ANAL/JET/CDFR/5636

December 21st, 2001

Version 4.5

Comparison of the Isolated Direct Photon Cross Sections in $p\bar{p}$ Collisions at $\sqrt{s} = 1.8$ TeV and $\sqrt{s} = 0.63$ TeV

D. Acosta,[12] T. Affolder,[23] H. Akimoto,[45] A. Akopian,[37] M. G. Albrow,[11] P. Amaral,[8] D. Amidei,[25] K. Anikeev,[24] J. Antos,[1] G. Apollinari,[11] T. Arisawa,[45] A. Artikov,[9] T. Asakawa,[43] W. Ashmanskas,[8] F. Azfar,[30] P. Azzi-Bacchetta,[31] N. Bacchetta,[31] H. Bachacou,[23] S. Bailey,[16] P. de Barbaro,[36] A. Barbaro-Galtieri,[23] V. E. Barnes,[35] B. A. Barnett,[19] S. Baroiant,[5] M. Barone,[13] G. Bauer,[24] F. Bedeschi,[33] S. Belforte,[42] W. H. Bell,[15] G. Bellettini,[33] J. Bellinger,[46] D. Benjamin,[10] J. Bensinger,[4] A. Beretvas,[11] J. P. Berge,[11] J. Berryhill,[8] A. Bhatti,[37] M. Binkley,[11] D. Bisello,[31] M. Bishai,[11] R. E. Blair,[2] C. Blocker,[4] K. Bloom,[25] B. Blumenfeld,[19] S. R. Blusk,[36] A. Bocci,[37] A. Bodek,[36] W. Bokhari,[32] G. Bolla,[35] Y. Bonushkin,[6] D. Bortoletto,[35] J. Boudreau,[34] A. Brandl,[27] S. van den Brink,[19] C. Bromberg,[26] M. Brozovic,[10] E. Brubaker,[23] N. Bruner,[27] E. Buckley-Geer,[11] J. Budagov,[9] H. S. Budd,[36] K. Burkett,[16] G. Busetto,[31] A. Byon-Wagner,[11] K. L. Byrum,[2] S. Cabrera,[10] P. Calafiura,[23] M. Campbell,[25]

W. Carithers,[23] J. Carlson,[25] D. Carlsmith,[46] W. Caskey,[5] A. Castro,[3] D. Cauz,[42]
A. Cerri,[33] A. W. Chan,[1] P. S. Chang,[1] P. T. Chang,[1] J. Chapman,[25] C. Chen,[32]
Y. C. Chen,[1] M. -T. Cheng,[1] M. Chertok,[5] G. Chiarelli,[33] I. Chirikov-Zorin,[9]
G. Chlachidze,[9] F. Chlebana,[11] L. Christofek,[18] M. L. Chu,[1] Y. S. Chung,[36]
C. I. Ciobanu,[28] A. G. Clark,[14] A. P. Colijn,[11] A. Connolly,[23] J. Conway,[38] M. Cordelli,[13]
J. Cranshaw,[40] R. Cropp,[41] R. Culbertson,[11] D. Dagenhart,[44] S. D'Auria,[15] F. DeJongh,[11]
S. Dell'Agnello,[13] M. Dell'Orso,[33] S. Demers,[37] L. Demortier,[37] M. Deninno,[3]
P. F. Derwent,[11] T. Devlin,[38] J. R. Dittmann,[11] A. Dominguez,[23] S. Donati,[33] J. Done,[39]
M. D'Onofrio,[33] T. Dorigo,[16] N. Eddy,[18] K. Einsweiler,[23] J. E. Elias,[11] E. Engels, Jr.,[34]
R. Erbacher,[11] D. Errede,[18] S. Errede,[18] Q. Fan,[36] H.-C. Fang,[23] R. G. Feild,[47]
J. P. Fernandez,[11] C. Ferretti,[33] R. D. Field,[12] I. Fiori,[3] B. Flaugher,[11] G. W. Foster,[11]
M. Franklin,[16] J. Freeman,[11] J. Friedman,[24] Y. Fukui,[22] I. Furic,[24] S. Galeotti,[33]
A. Gallas,[(**)] [16] M. Gallinaro,[37] T. Gao,[32] M. Garcia-Sciveres,[23] A. F. Garfinkel,[35]
P. Gatti,[31] C. Gay,[47] D. W. Gerdes,[25] P. Giannetti,[33] P. Giromini,[13] V. Glagolev,[9]
D. Glenzinski,[11] M. Gold,[27] J. Goldstein,[11] I. Gorelov,[27] A. T. Goshaw,[10] Y. Gotra,[34]
K. Goulianos,[37] C. Green,[35] G. Grim,[5] P. Gris,[11] L. Groer,[38] C. Grosso-Pilcher,[8]
M. Guenther,[35] G. Guillian,[25] J. Guimaraes da Costa,[16] R. M. Haas,[12] C. Haber,[23]
S. R. Hahn,[11] C. Hall,[16] T. Handa,[17] R. Handler,[46] W. Hao,[40] F. Happacher,[13] K. Hara,[43]
A. D. Hardman,[35] R. M. Harris,[11] F. Hartmann,[20] K. Hatakeyama,[37] J. Hauser,[6]
J. Heinrich,[32] A. Heiss,[20] M. Herndon,[19] C. Hill,[5] A. Hocker,[36] K. D. Hoffman,[35] C. Holck,[32]
R. Hollebeek,[32] L. Holloway,[18] B. T. Huffman,[30] R. Hughes,[28] J. Huston,[26] J. Huth,[16]

H. Ikeda,[43] J. Incandela,[(***) 11] G. Introzzi,[33] A. Ivanov,[36] J. Iwai,[45] Y. Iwata,[17] E. James,[25] M. Jones,[32] U. Joshi,[11] H. Kambara,[14] T. Kamon,[39] T. Kaneko,[43] K. Karr,[44] S. Kartal,[11] H. Kasha,[47] Y. Kato,[29] T. A. Keaffaber,[35] K. Kelley,[24] M. Kelly,[25] D. Khazins,[10] T. Kikuchi,[43] B. Kilminster,[36] B. J. Kim,[21] D. H. Kim,[21] H. S. Kim,[18] M. J. Kim,[21] S. B. Kim,[21] S. H. Kim,[43] Y. K. Kim,[23] M. Kirby,[10] M. Kirk,[4] L. Kirsch,[4] S. Klimenko,[12] P. Koehn,[28] K. Kondo,[45] J. Konigsberg,[12] A. Korn,[24] A. Korytov,[12] E. Kovacs,[2] J. Kroll,[32] M. Kruse,[10] S. E. Kuhlmann,[2] K. Kurino,[17] T. Kuwabara,[43] A. T. Laasanen,[35] N. Lai,[8] S. Lami,[37] S. Lammel,[11] J. Lancaster,[10] M. Lancaster,[23] R. Lander,[5] A. Lath,[38] G. Latino,[33] T. LeCompte,[2] A. M. Lee IV,[10] K. Lee,[40] S. Leone,[33] J. D. Lewis,[11] M. Lindgren,[6] T. M. Liss,[18] J. B. Liu,[36] Y. C. Liu,[1] D. O. Litvintsev,[11] O. Lobban,[40] N. Lockyer,[32] J. Loken,[30] M. Loreti,[31] D. Lucchesi,[31] P. Lukens,[11] S. Lusin,[46] L. Lyons,[30] J. Lys,[23] R. Madrak,[16] K. Maeshima,[11] P. Maksimovic,[16] L. Malferrari,[3] M. Mangano,[33] M. Mariotti,[31] G. Martignon,[31] A. Martin,[47] J. A. J. Matthews,[27] J. Mayer,[41] P. Mazzanti,[3] K. S. McFarland,[36] P. McIntyre,[39] E. McKigney,[32] M. Menguzzato,[31] A. Menzione,[33] P. Merkel,[11] C. Mesropian,[37] A. Meyer,[11] T. Miao,[11] R. Miller,[26] J. S. Miller,[25] H. Minato,[43] S. Miscetti,[13] M. Mishina,[22] G. Mitselmakher,[12] Y. Miyazaki,[29] N. Moggi,[3] E. Moore,[27] R. Moore,[25] Y. Morita,[22] T. Moulik,[35] M. Mulhearn,[24] A. Mukherjee,[11] T. Muller,[20] A. Munar,[33] P. Murat,[11] S. Murgia,[26] J. Nachtman,[6] V. Nagaslaev,[40] S. Nahn,[47] H. Nakada,[43] I. Nakano,[17] C. Nelson,[11] T. Nelson,[11] C. Neu,[28] D. Neuberger,[20] C. Newman-Holmes,[11] C.-Y. P. Ngan,[24] H. Niu,[4] L. Nodulman,[2] A. Nomerotski,[12] S. H. Oh,[10] Y. D. Oh,[21] T. Ohmoto,[17] T. Ohsugi,[17] R. Oishi,[43] T. Okusawa,[29] J. Olsen,[46]

W. Orejudos,[23] C. Pagliarone,[33] F. Palmonari,[33] R. Paoletti,[33] V. Papadimitriou,[40] D. Partos,[4] J. Patrick,[11] G. Pauletta,[42] M. Paulini,[(*) 23] C. Paus,[24] D. Pellett,[5] L. Pescara,[31] T. J. Phillips,[10] G. Piacentino,[33] K. T. Pitts,[18] A. Pompos,[35] L. Pondrom,[46] G. Pope,[34] M. Popovic,[41] F. Prokoshin,[9] J. Proudfoot,[2] F. Ptohos,[13] O. Pukhov,[9] G. Punzi,[33] A. Rakitine,[24] F. Ratnikov,[38] D. Reher,[23] A. Reichold,[30] P. Renton,[30] A. Ribon,[31] W. Riegler,[16] F. Rimondi,[3] L. Ristori,[33] M. Riveline,[41] W. J. Robertson,[10] A. Robinson,[41] T. Rodrigo,[7] S. Rolli,[44] L. Rosenson,[24] R. Roser,[11] R. Rossin,[31] C. Rott,[35] A. Roy,[35] A. Ruiz,[7] A. Safonov,[5] R. St. Denis,[15] W. K. Sakumoto,[36] D. Saltzberg,[6] C. Sanchez,[28] A. Sansoni,[13] L. Santi,[42] H. Sato,[43] P. Savard,[41] A. Savoy-Navarro,[11] P. Schlabach,[11] E. E. Schmidt,[11] M. P. Schmidt,[47] M. Schmitt,[(**) 16] L. Scodellaro,[31] A. Scott,[6] A. Scribano,[33] S. Segler,[11] S. Seidel,[27] Y. Seiya,[43] A. Semenov,[9] F. Semeria,[3] T. Shah,[24] M. D. Shapiro,[23] P. F. Shepard,[34] T. Shibayama,[43] M. Shimojima,[43] M. Shochet,[8] A. Sidoti,[31] J. Siegrist,[23] A. Sill,[40] P. Sinervo,[41] P. Singh,[18] A. J. Slaughter,[47] K. Sliwa,[44] C. Smith,[19] F. D. Snider,[11] A. Solodsky,[37] J. Spalding,[11] T. Speer,[14] P. Sphicas,[24] F. Spinella,[33] M. Spiropulu,[8] L. Spiegel,[11] J. Steele,[46] A. Stefanini,[33] J. Strologas,[18] F. Strumia, [14] D. Stuart,[11] K. Sumorok,[24] T. Suzuki,[43] T. Takano,[29] R. Takashima,[17] K. Takikawa,[43] P. Tamburello,[10] M. Tanaka,[43] B. Tannenbaum,[6] M. Tecchio,[25] R. Tesarek,[11] P. K. Teng,[1] K. Terashi,[37] S. Tether,[24] A. S. Thompson,[15] R. Thurman-Keup,[2] P. Tipton,[36] S. Tkaczyk,[11] D. Toback,[39] K. Tollefson,[36] A. Tollestrup,[11] D. Tonelli,[33] H. Toyoda,[29] W. Trischuk,[41] J. F. de Troconiz,[16] J. Tseng,[24] D. Tsybychev,[11] N. Turini,[33] F. Ukegawa,[43] T. Vaiciulis,[36] J. Valls,[38] S. Vejcik III,[11] G. Velev,[11] G. Veramendi,[23] R. Vidal,[11] I. Vila,[7]

R. Vilar,[7] I. Volobouev,[23] M. von der Mey,[6] D. Vucinic,[24] R. G. Wagner,[2] R. L. Wagner,[11] N. B. Wallace,[38] Z. Wan,[38] C. Wang,[10] M. J. Wang,[1] B. Ward,[15] S. Waschke,[15] T. Watanabe,[43] D. Waters,[30] T. Watts,[38] R. Webb,[39] H. Wenzel,[20] W. C. Wester III,[11] A. B. Wicklund,[2] E. Wicklund,[11] T. Wilkes,[5] H. H. Williams,[32] P. Wilson,[11] B. L. Winer,[28] D. Winn,[25] S. Wolbers,[11] D. Wolinski,[25] J. Wolinski,[26] S. Wolinski,[25] S. Worm,[27] X. Wu,[14] J. Wyss,[33] W. Yao,[23] G. P. Yeh,[11] P. Yeh,[1] J. Yoh,[11] C. Yosef,[26] T. Yoshida,[29] I. Yu,[21] S. Yu,[32] Z. Yu,[47] A. Zanetti,[42] F. Zetti,[23] and S. Zucchelli[3]

(CDF Collaboration)

[1] *Institute of Physics, Academia Sinica, Taipei, Taiwan 11529, Republic of China*

[2] *Argonne National Laboratory, Argonne, Illinois 60439*

[3] *Istituto Nazionale di Fisica Nucleare, University of Bologna, I-40127 Bologna, Italy*

[4] *Brandeis University, Waltham, Massachusetts 02254*

[5] *University of California at Davis, Davis, California 95616*

[6] *University of California at Los Angeles, Los Angeles, California 90024*

[7] *Instituto de Fisica de Cantabria, CSIC-University of Cantabria, 39005 Santander, Spain*

[8] *Enrico Fermi Institute, University of Chicago, Chicago, Illinois 60637*

[9] *Joint Institute for Nuclear Research, RU-141980 Dubna, Russia*

[10] *Duke University, Durham, North Carolina 27708*

[11] *Fermi National Accelerator Laboratory, Batavia, Illinois 60510*

[12] *University of Florida, Gainesville, Florida 32611*

[13] *Laboratori Nazionali di Frascati, Istituto Nazionale di Fisica Nucleare, I-00044 Frascati, Italy*

[14] *University of Geneva, CH-1211 Geneva 4, Switzerland*

[15] *Glasgow University, Glasgow G12 8QQ, United Kingdom*

[16] *Harvard University, Cambridge, Massachusetts 02138*

[17] *Hiroshima University, Higashi-Hiroshima 724, Japan*

[18] *University of Illinois, Urbana, Illinois 61801*

[19] *The Johns Hopkins University, Baltimore, Maryland 21218*

[20] *Institut für Experimentelle Kernphysik, Universität Karlsruhe, 76128 Karlsruhe, Germany*

[21] *Center for High Energy Physics: Kyungpook National University, Taegu 702-701; Seoul National University, Seoul 151-742; and SungKyunKwan University, Suwon 440-746; Korea*

[22] *High Energy Accelerator Research Organization (KEK), Tsukuba, Ibaraki 305, Japan*

[23] *Ernest Orlando Lawrence Berkeley National Laboratory, Berkeley, California 94720*

[24] *Massachusetts Institute of Technology, Cambridge, Massachusetts 02139*

[25] *University of Michigan, Ann Arbor, Michigan 48109*

[26] *Michigan State University, East Lansing, Michigan 48824*

[27] *University of New Mexico, Albuquerque, New Mexico 87131*

[28] *The Ohio State University, Columbus, Ohio 43210*

[29] *Osaka City University, Osaka 588, Japan*

[30] *University of Oxford, Oxford OX1 3RH, United Kingdom*

[31] *Universita di Padova, Istituto Nazionale di Fisica Nucleare, Sezione di Padova, I-35131 Padova, Italy*

[32] *University of Pennsylvania, Philadelphia, Pennsylvania 19104*

[33] *Istituto Nazionale di Fisica Nucleare, University and Scuola Normale Superiore of Pisa, I-56100 Pisa, Italy*

[34] *University of Pittsburgh, Pittsburgh, Pennsylvania 15260*

[35] *Purdue University, West Lafayette, Indiana 47907*

[36] *University of Rochester, Rochester, New York 14627*

[37] *Rockefeller University, New York, New York 10021*

[38] *Rutgers University, Piscataway, New Jersey 08855*

[39] *Texas A&M University, College Station, Texas 77843*

[40] *Texas Tech University, Lubbock, Texas 79409*

[41] *Institute of Particle Physics, University of Toronto, Toronto M5S 1A7, Canada*

[42] *Istituto Nazionale di Fisica Nucleare, University of Trieste/ Udine, Italy*

[43] *University of Tsukuba, Tsukuba, Ibaraki 305, Japan*

[44] *Tufts University, Medford, Massachusetts 02155*

[45] *Waseda University, Tokyo 169, Japan*

[46] *University of Wisconsin, Madison, Wisconsin 53706*

[47] *Yale University, New Haven, Connecticut 06520*

(*) *Now at Carnegie Mellon University, Pittsburgh, Pennsylvania 15213*

(**) *Now at Northwestern University, Evanston, Illinois 60208*

(***) *Now at University of California, Santa Barbara, CA 93106*

Abstract

We have measured the cross sections $d^2\sigma/dP_T d\eta$ for production of isolated direct photons in $p\bar{p}$ collisions at two different center-of-mass energies, 1.8 TeV and 0.63 TeV, using the Collider Detector at Fermilab (CDF). The normalization of both data sets agree with the predictions of Quantum Chromodynamics (QCD) for photon transverse momentum (P_T) of 25 GeV/c, but the shapes versus photon P_T do not. These shape differences lead to a significant disagreement in the ratio of cross sections in the scaling variable $x_T(\equiv 2P_T/\sqrt{s})$. This disagreement in the x_T ratio is difficult to explain with conventional theoretical uncertainties such as scale dependence and parton distribution parameterizations.

1 Introduction

In this article we present a measurement of the cross section for production of isolated prompt photons in proton-antiproton collisions at center-of-mass energies $\sqrt{s} = 1.8$ TeV and $\sqrt{s} = 0.63$ TeV using the Collider Detector at Fermilab (CDF). Prompt photons are those produced in the $p\bar{p}$ collision, in distinction from the copious background of photons produced by decays of hadrons such as the π^0 and η mesons. In Quantum Chromodynamics (QCD), at lowest order, prompt photon production is dominated by the Compton process $gq \to \gamma q$, which is sensitive to the gluon distribution of the proton [1]. This process has been previously measured by the CDF collaboration at $\sqrt{s}$= 1.8 TeV [2, 3]; a difference between the data and the theory was observed in the shape of the differential cross section versus photon P_T. The discrepancy could possibly be eliminated by a change in the gluon distribution inside the proton [4]. In this analysis the photon cross section has been measured using the same detector and the same technique at two widely different center-of-mass energies, with a larger data sample than that of the previous measurement. A comparison of the ratio of the two cross sections provides a precise test of the QCD calculations, as many of the experimental uncertainties cancel. The cross section ratio also provides a direct probe of the QCD matrix elements, as the theoretical uncertainties due to the gluon distribution are reduced.

2 Detector Description and Event Selection

A detailed description of the CDF detector may be found in Refs. [3, 5]. Here we describe the two detector systems used to distinguish prompt photons from neutral hadron backgrounds. A multiwire proportional chamber with cathode strip readout (the Central Electromagnetic Strip system, CES) embedded in each central electromagnetic calorimeter (CEM) module measures the transverse profile of the electromagnetic shower at a depth of approximately 6 radiation lengths. In front of each CEM module, a similar multiwire chamber (the Central Preradiator, CPR) samples electromagnetic showers that begin in the coil of the solenoid magnet.

The photon trigger used to acquire these data consists of three levels [6]. At the first level, a single trigger tower [7] in the CEM is required to be above a threshold, typically $P_T > 8$ GeV/c. The second trigger level finds clusters of transverse energy among the trigger towers in the calorimeter, and requires that 88% of the cluster transverse energy be in the electromagnetic (EM) compartment of the calorimeter. In addition, the Level 2 electronics require that the transverse energy in the 3×3 grid of trigger towers surrounding the photon candidate (equivalent to a radius $R = \sqrt{(\Delta\eta)^2 + (\Delta\phi)^2} = 0.4$) is less than 4 GeV, thereby requiring the photon to be *isolated* [8]. In the third level of the trigger, software algorithms require a CES cluster of energy of more than 0.5 GeV. This cluster determines the position of the photon; fiducial cuts are then applied to avoid uninstrumented regions of the detector. In both the second and third trigger levels, P_T thresholds are applied. The data set at 1.8 TeV was selected by a prescaled [9] trigger with a threshold of $P_T > 10$ GeV/c, an

unprescaled trigger with a threshold of $P_T > 23$ GeV/c, and an unprescaled trigger with a threshold of $P_T > 50$ GeV/c without the isolation cut. The 0.63 TeV data were acquired with an unprescaled trigger with a threshold of $P_T > 6$ GeV/c. The respective integrated luminosities for the 1.8 TeV data are 84, 84, and 1.1 pb^{-1} for the 50, 23, and 10 GeV/c thresholds, and 0.54 pb^{-1} for the 0.63 TeV sample.

The selection of prompt photon candidates from the triggered events is essentially the same as those used previously [3], with a minor change in the isolation cut [10]. The selection cuts, cut efficiencies, and systematic uncertainties are listed in Table 1. Candidates are rejected if there is a reconstructed charged track with P_T greater than approximately 0.4 GeV/c pointing at the EM cluster or the CPR chamber containing the photon. To improve the signal/background ratio, the isolation cut applied in the trigger is tightened to require less than 1 GeV of transverse energy in a cone radius of 0.4. After these selections, the main backgrounds to the prompt photons are from single π^0 and η mesons, with smaller backgrounds from multiple π^0's. These backgrounds are reduced by requiring there be no other photon candidate above 1 GeV energy in the CES chamber containing the photon candidate. The total acceptance-times-efficiency for prompt photons within $|\eta| < 0.9$ is approximately 34% for the 1.8 TeV data and approximately 37% for the 0.63 TeV data (see Table 1).

3 Background subtraction

We employ two methods for statistically subtracting the remaining neutral meson background from the photon candidates: the *conversion method* counts the fraction of photon conversions ($\gamma \to e^+e^-$) in the material of the magnet coil by using the CPR, and the *profile method* uses the transverse profile of the electromagnetic shower in the CES. For the conversion method, the probability of a single photon conversion is approximately 60%, while that for the two-photon decay of a π^0 or η is larger, approximately 86%. For the profile method, the transverse profile of the electromagnetic shower of each photon candidate is compared to that measured for electrons in a test beam in the same momentum range. On a statistical basis, a measure of the goodness of fit (labeled $\tilde{\chi}^2$since the distribution for single photons is approximately a χ^2 distribution) is expected to be larger for a neutral meson decaying to two photons than for a single photon because a neutral meson usually produces a wider EM shower [2]. At 20 GeV/c approximately 80% of the single photons and 40% of the background have a $\tilde{\chi}^2$ less than 4. The conversion method has the advantage of an unlimited P_T range and smaller systematic uncertainties in the shape of the cross section as a function of photon P_T. The profile method has the advantage of a better separation of signal and background than the conversion method in the low P_T region, where the two photons from π^0 decay have a larger spatial separation.

For both background subtraction methods, the number of photons (N_γ) in a bin of P_T is obtained from the number of photon candidates (N), the fraction of photon candidates that pass a fixed cut defined below (ϵ), and the corresponding fractions for true photons (ϵ_γ) and

background (ϵ_b), using:

$$N_\gamma = \left(\frac{\epsilon - \epsilon_b}{\epsilon_\gamma - \epsilon_b} \right) N \tag{1}$$

Equation 1 comes from $\epsilon N = \epsilon_\gamma N_\gamma + \epsilon_b N_b$ with $N_b = N - N_\gamma$. For the conversion method, ϵ is the fraction of photon candidates which produce a pulse height in the CPR greater than 1 minimum ionizing particle, within a 66 milliradian "window" (5 channels) centered on the photon direction in ϕ. For the profile method, ϵ is the fraction of events which have $\tilde{\chi}^2 < 4$ out of all events with $\tilde{\chi}^2 < 20$. Using these methods, we measure the signal/background ratio bin-by-bin and propagate the statistical uncertainty of each bin into the cross section measurement, including the effect of the background subtraction.

The signal and background efficiencies for the two methods are similar to the previous analyses [2, 3]. For the profile method ϵ_γ and ϵ_b are the same as those used in reference [2]. For the conversion method ϵ_γ is estimated from the following equation:

ϵ_γ = 1 - exp(-7t/9)

where t is the amount of material in radiation lengths in front of the CPR. Corrections to this estimate of ϵ_γ are made on an event-by-event basis for the amount of material traversed, as well as changes in the pair production cross section with photon energy [11]. An additional correction is made for photon showers that begin after the photon has passed through the CPR, but in which a soft photon or electron from the shower is scattered backwards at a large angle and gives a CPR signal. This correction is estimated with an electromagnetic shower simulation [12]. The final correction, estimated using non-isolated photon triggers, is due to CPR signals arising from soft photons from the underlying event or additional $\bar{p}p$

interactions (pileup). With the higher luminosity of the current data sample, the number of pileup events increased; hence, this correction is the main difference between the current and previous analyses [3]. All of the corrections to ϵ_γ are applied to ϵ_b as well. In addition ϵ_b is corrected for the multiple photons from background:

$$\epsilon_b = 1 - \exp(-7/9 * t * N_\gamma(P_T)).$$

The function $N_\gamma(P_T)$ is the average number of photons within the CPR "window" defined earlier. This changes with transverse momentum and particle type and is estimated using a detector simulation of π^0, η and K^0_S mesons with a relative production ratio of 1:1:0.4 [2].

The two methods developed to check the measured number of photons in the previous analysis [3] are repeated in this analysis. The most important of these is the comparison of the number of photons determined by the conversion and profile methods in the region of photon P_T where both methods are valid. The two methods should agree within their independent systematic uncertainties, estimated in the previous analysis to be 20% for the profile method and 10% for the conversion method for photon P_T of 20 GeV/c. The two methods agreed to within 2% in the previous analysis [3], much better than expected given the systematic uncertainties. In the current analysis, before recalibration, the conversion method measurement of the photon cross section is 20% smaller than the profile method measurement at P_T=20 GeV/c.

The second method developed to check the two background subtraction methods uses reconstructed $\rho^\pm$ mesons (Figure 1). Charged pions from the ρ meson decays are required to fall in a separate calorimeter module from the neutral pions, which then provide a clean

probe of the photon measurement techniques, in particular ϵ_b. There was excellent agreement between the measured and expected efficiencies in the ρ meson peak region in the previous analysis. There is also good agreement in the current profile method analysis, independently checked in the 1.8 TeV and 0.63 TeV data samples. For example, in the 1.8 TeV sample the measured efficiency for the ρ meson is 0.461 ± 0.010, and the expected value is 0.464. For the current conversion method analysis, however, there is a significant difference between the measured and expected hit rates, and the difference is identical in the 1.8 TeV and 0.63 TeV reconstructed ρ meson data sets. The measured conversion rate is $0.868 \pm .007$ (0.814 ± 0.008), and the expected value is 0.835 ± 0.006 (0.781 ± 0.006) in the 1.8 (0.63) TeV ρ meson data sample. After ϵ_b has been changed to agree with the measured hit rate from the ρ meson sample, the the profile method and conversion method cross sections agree to within 10% at P_T=20 GeV/c. The precise cause of this difference is not understood, and its effect on the conversion method signal efficiency is unknown. Therefore, we use the profile method cross section normalization at low P_T to estimate the appropriate change in conversion method signal efficiency. Hence, in this analysis the profile method determines the overall cross section normalization while the conversion method determines the cross section shape versus photon P_T. This utilizes the strengths of each method for the combined cross section result. Further discussion of the photon background subtraction in this analysis can be found in the Appendix.

Using the procedure outlined above, the purity of the sample (number of photons/number of candidate events) is shown in Figure 2 as a function of photon P_T for the 1.8 TeV and 0.63

TeV data sets, as well as for the previous 1.8 TeV analysis [3]. The purity improves with increasing P_T as expected from the enhanced effectiveness of the isolation cuts in reducing jet backgrounds. The differences in photon fraction at high P_T between the two 1.8 TeV analyses may be due to changes in the number of background events due to differing isolation cuts. Understanding such subtle effects in jet fragmentation is beyond the scope of this paper, and the fraction of background events in a particular sample does not affect the prompt photon signal itself.

4 Experimental systematic uncertainties

The systematic uncertainties in the cross section normalization and shape are dominated by uncertainties in ϵ_γ and ϵ_b for the background subtraction method for both cross sections at a given P_T. The largest impact on the physics results presented later in this article would be a systematic effect on the shape of the cross section as a function of photon P_T. Despite the difficulties with the conversion method normalization, the shape of the measured cross section is well determined. For example, the uncertainty due to the choice of ϵ_γ in the conversion method (as discussed in the Appendix) leads to a 12% normalization uncertainty but only a 5% change in slope between photon P_T values of 11 GeV/c to 115 GeV/c. The second uncertainty in ϵ_γ and ϵ_b comes from the correction for possible CPR hits from backscattered low energy photons and electrons in the electromagnetic calorimeter shower. This is estimated with a detector simulation [12] to be 1.6% at 9 GeV/c and 6% at 100 GeV/c. The uncertainty in the composition of the background [2] leads to a cross

section uncertainty of 12% at 9 GeV/c and 0.4% at 100 GeV/c. The entire mix of background sources is checked by a sample of events passing the same photon cuts as the data, with the exception of a slightly relaxed isolation cut. This shows agreement with expectations within the uncertainty on ϵ_b quoted above. Finally, there are additional (correlated) uncertainties due to luminosity (4.1% at 1.8 TeV and 4.4% at 0.63 TeV), trigger efficiencies (2.2% at 9 GeV/c and 5.4% at 50 GeV/c), selection efficiencies (3.6% at 1.8 TeV and 6.2% at 0.63 TeV), and photon energy scale (4.5%).

5 Cross section evaluation and comparison to QCD models

From the number of prompt photons in a given bin of transverse momentum, along with the acceptance and the integrated luminosity for that bin, the isolated prompt photon cross section is derived and tabulated in Tables 2 and 3. Also tabulated are the number of events (photon candidates), the number of photons after the background subtraction, and the statistical and systematic uncertainties. The systematic uncertainties listed are approximately 100% correlated bin-to-bin and include all normalization uncertainties.

In Figure 3 measurements from both data sets are compared to a next-to-leading order QCD calculation [13] derived using the CTEQ5M parton distributions [14] and $\mu = P_T$ for the renormalization, factorization, and fragmentation scales. The QCD prediction agrees qualitatively with the measurements over more than 4 orders of magnitude in cross section.

Figure 4a shows a comparison of the cross sections as a function of photon P_T and Figure 4b shows a comparison of the cross sections as a function of the scaling variable $x_T(\equiv 2P_T/\sqrt{s})$. The shape of the cross sections versus P_T (or x_T) is generally steeper than that of the theoretical predictions. Many variations of modern parton distributions and scales were tried, with small changes in the shape of the predictions, but none accurately predicted the shape of the cross sections, as seen in Figure 5. It is still possible other changes in the theory parameters could improve the agreement between data and theory for one or the other data sets. However, the comparison of the two cross sections as a function of photon x_T, a ratio in which most experimental and theoretical uncertainties cancel, is more difficult to reconcile with the NLO QCD calculations. The parton distributions at a fixed value of x_T are the same for 1.8 TeV and 0.63 TeV center-of-mass energies, except for changes due to QCD evolution which are very similar for different parton distribution parameterizations. In the region where the 1.8 TeV and 0.63 TeV data sets overlap in x_T, the variation of the 0.63 TeV/1.8 TeV cross section ratio with parton distribution [15] is 1%, and the variation with scale (between μ=P_T and μ=$P_T/2$) is only 4%. The experimental systematic uncertainties are also smaller in the x_T ratio, with the quadrature sum of the uncertainties in the 0.63 TeV/1.8 TeV ratio reduced to 10% at x_T=0.03 and 5% at x_T=0.15. The measured ratio of cross sections, however, is more than 50% larger than that predicted by NLO QCD (the ratio of data points shown in Figure 4b), and the disagreement is essentially independent of x_T in the range where 1.8 TeV and 0.63 TeV data sets overlap. The ratio is more than four standard deviations larger than that predicted by current NLO QCD calculations. These

results are reinforced when the CDF cross sections are compared to the results of the D0 and UA2 experiments [17, 18] as shown in Figure 6. There is excellent agreement between the CDF and UA2 data sets. The CDF and D0 data sets differ in normalization by about 20%, consistent with the quoted correlated systematic uncertainties of the measurements. The correlated systematic uncertainties of the D0 measurement are 10% at large P_T growing to 74% in the lowest P_T bin. CDF's correlated systematic uncertainties are listed in Tables 2 and 3, and are 11% at large P_T growing to 18% in the lowest P_T bin. Recently the D0 experiment has published a measurement of the photon cross section at 0.63 TeV, as well as the ratio of 0.63 TeV and 1.8 TeV cross sections [19]. In the D0 ratio measurement the lowest x_T points are systematically higher than NLO QCD, but the deviations are not significant in light of the combined statistical and systematic uncertainties.

One possibility for the observed discrepancy with NLO QCD is the lack of a complete description of the initial state parton shower in the NLO QCD calculation, which could give a recoil effect to the photon+jet system ("k_T"). Higher order QCD calculations including such effects are becoming available [20], but are not ready for detailed comparisons at this time. To explore qualitatively the effect of k_T on the comparisons, we have added a simplified gaussian smearing to the NLO QCD calculations to see if the measurements could be sensitive to these effects. The photon+jet system was given a transverse momentum recoil consistent with that measured in the Drell-Yan process at each center-of-mass energy (3 GeV at 0.63 TeV and 4 GeV at 1.8 TeV). The comparisons with the measurements are improved with the addition of these amounts of k_T. For example, the measured ratio of cross sections versus x_T

is only 19% larger than NLO QCD + k_T, compared to the 50% excess without k_T discussed earlier. We look forward to the maturation of the QCD calculations including the recoil effect due to soft gluon radiation.

6 Acknowledgments

We would like to thank Werner Vogelsang for providing the theoretical calculations used in this paper. We also thank the Fermilab staff and the technical staffs of the participating institutions for their vital contributions. This work was supported by the U.S. Department of Energy and National Science Foundation; the Italian Istituto Nazionale di Fisica Nucleare; the Ministry of Education, Science, Sports and Culture of Japan; the Natural Sciences and Engineering Research Council of Canada; the National Science Council of the Republic of China; the Swiss National Science Foundation; the A. P. Sloan Foundation; the Bundesministerium fuer Bildung und Forschung, Germany; the Korea Science and Engineering Foundation (KoSEF), the Korea Research Foundation, and the Comision Interministerial de Ciencia y Tecnologia, Spain.

Appendix: Recalibration of the Photon Background Subtraction

As mentioned in the main text of this paper, a sample of reconstructed π^0s from charged ρ meson decays has been used to check the two techniques for subtracting photon backgrounds. The relatively pure measurements of π^0s agree well with expectations for the profile method, but do not for the conversion method, as shown in figure 7. The dashed line in this figure is the expected π^0 CPR signal rate in the ρ meson peak region, falling below the data. The signal rate is largely independent of measured mass, and sideband subtractions of the hit rate for various selected mass regions had no effect on this result. The three most likely sources for the conversion method discrepancy, which have been extensively investigated [21], are: 1) an underestimate of the correction for CPR hits from multiple $p\bar{p}$ collisions; 2) an underestimate of the material in front of the CPR chambers; 3) a change in CPR chamber performance compared to the 1992 analysis. Our analysis has shown that no single source is the likely cause of the discrepancy; it is perhaps a complicated mixture of multiple effects [21]. The ρ meson sample is therefore used to recalibrate the conversion method. When this recalibration is done by correcting for the difference in the measured and expected ρ meson conversion rates, agreement is restored between the conversion method and profile method photon cross section measurements at both 1.8 TeV and 0.63 TeV. To do this, however, one has to assume a correction for the signal efficiency as well as the background efficiency, since the two are usually correlated. The size of the signal efficiency correction depends on the source of the conversion method discrepancy. The most extreme choice for the change in signal efficiency, which comes from the assumption that the entire source of the discrepancy is multiple $p\bar{p}$

collisions, increases the conversion method normalization by 30% more than no correction at all. On the other hand, the profile method normalization is apparently very robust at low P_T. As an example, when the efficiencies in the profile method are changed based on the measured uncertainty in the ρ meson measurement, the cross section changes by only 5% at P_T =20 GeV/c. Therefore, in the final cross section measurement the two methods are combined based on their respective strengths. The profile method determines the normalization of the cross section at low P_T, while the conversion method determines the shape with photon P_T. This is accomplished by correcting the conversion method background efficiency directly with the ρ meson measurement, then choosing the signal efficiency that matches the profile method normalization at low P_T.

References

[1] U. Baur *et al.*, *"Report of the Working Group on Photon and Weak Boson Production."*, eprint: hep-ph/0005226, May 2000.

[2] F. Abe *et al.* (CDF Collaboration),Phys. Rev. **D 48,** 2998 (1993).

[3] F. Abe *et al.* (CDF Collaboration), Phys. Rev. Lett. **68,** 2734 (1992).

[4] W. Vogelsang and A. Vogt, Nucl. Phys. **B 453,** 370 (1995).

[5] F. Abe *et al.* (CDF Collaboration), Nucl. Inst. and Meth. **A 271**, 387 (1988), and the references therein. The angular coordinate system used within CDF is (θ, ϕ), where θ is

the polar angle relative to the proton beam as measured from the event vertex, and ϕ the azimuth. The pseudorapidity is defined as $\eta = -\ln\tan(\theta/2)$.

[6] D. Amidei *et al.*, Nucl. Instrum. Methods Phys. Res., Sect. A **269**, 51 (1988).

[7] The trigger towers consist of two calorimeter towers in the cenrtal region, covering $0.1 \times 15^\circ$ in $\eta - \phi$ space. A typical CEM photon trigger cluster consists of one trigger tower, although neighboring trigger towers with more than 1 GeV can be added, as well as *their* neighbors.

[8] This is a change from the Level 2 configuration used in Ref [3], in which a 5×5 array was used to isolate the photon.

[9] A prescaled trigger is one in which every Nth event is recorded, where N is an integer, called the prescale factor.

[10] The isolation cut used in this analysis measures energy in a cone of radius 0.4 around the photon candidate; a cone radius of 0.7 was used in Ref [3].

[11] Y. S. Tsai, Rev. Mod. Phys. **46,** 815 (1974).

[12] GEANT3, R. Brun, *et al.*, CERN DD/EE/84-1.

[13] M. Gluck *et al.*, Phys. Rev. Lett. **73**, 388 (1994).

[14] H.L. Lai *et al.* (CTEQ Collaboration), Euro. Phys. J. **C 12,** 375 (2000).

[15] The other parton distribution functions used for comparison were CTEQ5HJ [14], MRST-99 [16], and MRST-99 $g \uparrow$ [16].

[16] A.D. Martin, R.G. Roberts, W.J. Stirling, R.S. Thorne, Nucl. Phys. Proc. Suppl. **79,** 210 (1999).

[17] B. Abbott *et al.* (D0 Collaboration), Phys. Rev. Lett. **84,** 2786 (2000).

[18] J. Alitti *et al.* (UA2 Collaboration), Phy. Lett. **B 263**, 544 (1991).

[19] V.M. Abazov *et al.* (D0 Collaboration), Phys. Rev. Lett.**87,** 251805 (2001).

[20] E. Laenen, G. Sterman, and W. Vogelsang, Phys. Rev. Lett. **84,** 4296 (2000). C. Fink, Ph.D. thesis, Florida State University, 2001, eprint: hep-ph/0105276.

[21] D. Partos, Ph.D. thesis, Brandeis University, 2001.

	1.8 TeV		0.63 TeV	
Analysis Cut	Efficiency	Uncertainty	Efficiency	Uncertainty
Remove Uninstrumented Regions	0.977	0.010	0.977	0.010
Fiducial	0.64	0.000	0.64	0.000
$\|Z_{vertex}\| < 60$ cm	0.937	0.011	0.85	0.05
Isolation	0.832	0.004	0.919	0.013
No track	0.797	0.005	0.853	0.007
Energy in 2^{nd} CES cluster < 1 GeV	0.893	0.031	0.893	0.031
Missing E_T/E_T <0.8	0.976	0.014	0.976	0.014
Total	0.339	0.036	0.372	0.062

Table 1: A list of the photon selection efficiencies and their uncertainties for the 1.8 and 0.63 TeV data. The selection criteria and techniques used to measure their efficiencies are very similar to the previous analysis [3]. Several CES and CEM channels were not working and were removed. The 'fiducial' cuts require that the photon is not close to detector boundaries. The 'Z_{vertex}' cut requires the $\bar{p}p$ interaction point to be near the center of the detector. The 'isolation' cut requires that the transverse energy be less than 1 GeV in a cone of radius $R = \sqrt{(\Delta\eta)^2 + (\Delta\phi)^2} = 0.4$ around the photon direction. The 'no track' cut refers to events with a reconstructed track pointing at the CPR chamber containing the photon. The 'energy in a 2nd CES cluster' cut reduces backgrounds from neutral mesons. The 'missing E_T' cut removes photon candidates arising from cosmic rays.

$\sqrt{s} = 1.8$ TeV						
P_T	# Candidates	# Photons	$d^2\sigma/dP_T d\eta$	Stat.	Sys.	NLO QCD
(GeV/c)	N	N_γ	(pb/(GeV/c))	(%)	(%)	(pb/(GeV/c))
11.5	13818	3839	8.84×10^3	9.0	18.0	7.36×10^3
12.5	12809	4437	7.89×10^3	8.5	14.4	5.21×10^3
13.5	9304	3074	4.50×10^3	10.0	14.5	3.77×10^3
14.5	6173	1772	2.61×10^3	9.3	16.3	2.78×10^3
15.5	4150	1626	2.40×10^3	8.4	12.1	2.09×10^3
17.0	4993	2173	1.61×10^3	6.8	12.5	1.43×10^3
19.8	4133	1945	7.38×10^2	6.7	12.0	7.26×10^2
23.8	1410	809	3.12×10^2	9.3	11.3	3.24×10^2
27.9	38033	25226	1.55×10^2	3.5	10.5	1.63×10^2
31.0	13283	9171	9.64×10^1	2.6	10.5	1.01×10^2
33.9	16767	11885	6.32×10^1	2.3	10.8	6.75×10^1
37.9	9244	6750	3.69×10^1	3.0	10.8	4.06×10^1
41.9	5467	4210	2.33×10^1	3.7	10.8	2.57×10^1
48.9	6683	5453	1.14×10^1	3.3	11.3	1.25×10^1
62.4	3253	2376	3.12×10^0	4.8	10.2	3.96×10^0
80.8	924	686	8.21×10^{-1}	12.0	10.6	1.12×10^0
114.7	386	316	1.43×10^{-1}	13.0	11.4	1.89×10^{-1}

Table 2: The 1.8 TeV isolated photon cross section is tabulated along with the statistical and systematic uncertainties. The systematic uncertainties include normalization uncertainties and are approximately 100% correlated bin-to-bin. The column labeled NLO QCD is the result of the calculation discussed in [13].

$\sqrt{s} = 0.63$ TeV						
P_T	# Candidates	# Photons	$d^2\sigma/dP_T d\eta$	Stat.	Sys.	NLO QCD
(GeV/c)	N	N_γ	(pb/(GeV/c))	(%)	(%)	(pb/(GeV/c))
9.9	26606	6260	7.55×10^3	9.5	21.6	4.71×10^3
11.9	8531	2382	2.90×10^3	8.4	18.8	2.09×10^3
14.3	4048	1532	1.26×10^3	8.5	16.5	9.12×10^2
17.4	1269	590	4.89×10^2	11.9	15.6	3.83×10^2
20.8	550	302	1.92×10^2	15.0	15.0	1.66×10^2
25.7	245	125	5.40×10^1	23.0	14.9	6.11×10^1
33.6	112	84	2.03×10^1	25.2	14.8	1.61×10^1

Table 3: The 0.63 TeV isolated photon cross section calculated is tabulated along with the statistical and systematic uncertainties. The systematic uncertainties include normalization uncertainties and are approximately 100% correlated bin-to-bin. The column labeled NLO QCD is the result of the calculation discussed in [13].

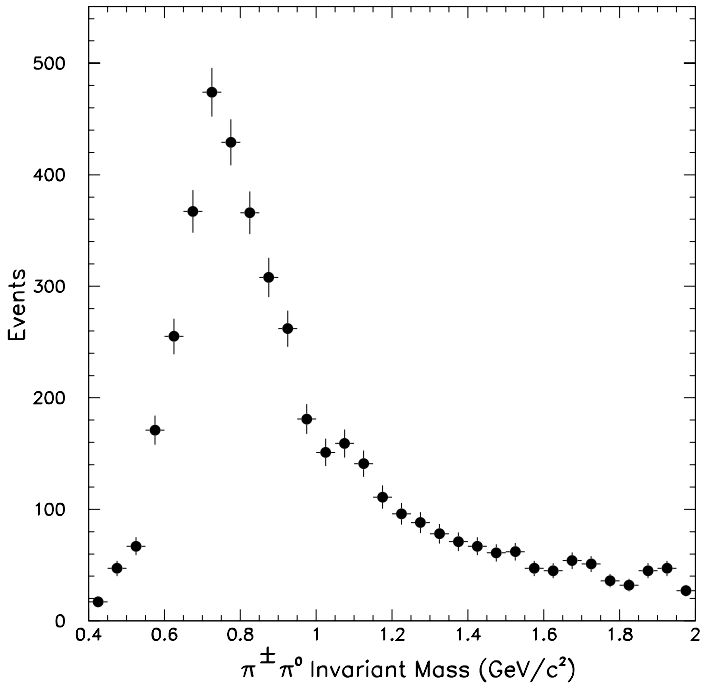

Figure 1: The $\rho^{\pm}$ data sample used to calibrate the profile and conversion methods. Fits to the mass distribution using a Breit-Wigner line shape, plus a flat background component, failed to describe the data. A gaussian fit to the truncated peak region gave a fitted mass of 0.767 GeV, consistent with the PDG ρ meson mass. As discussed in the appendix, a fit is not used in the analysis since the conversion method hit rate is the same for the signal and background dominated regions.

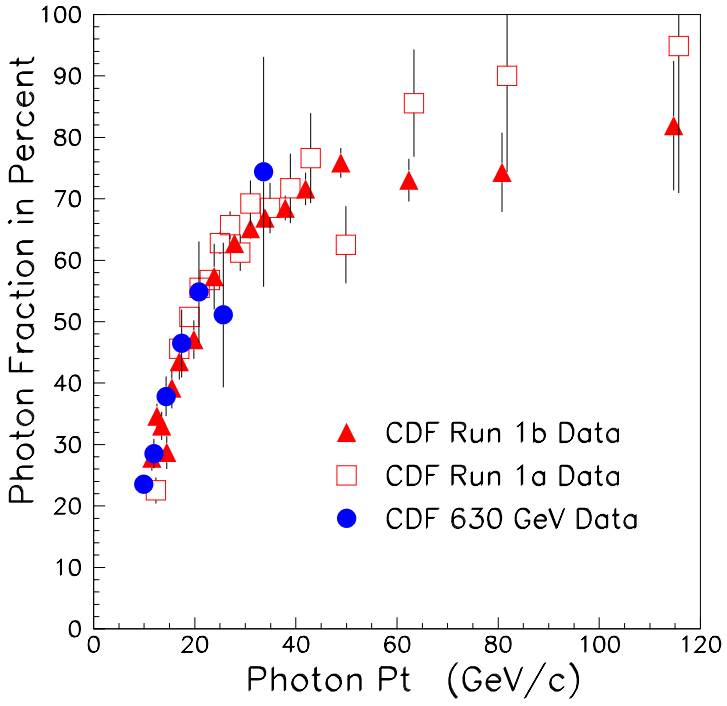

Figure 2: The photon fractions (ratio of the number of prompt photons to the number of prompt photon candidates) at the two different center-of-mass energies, and from the last published CDF analysis [3].

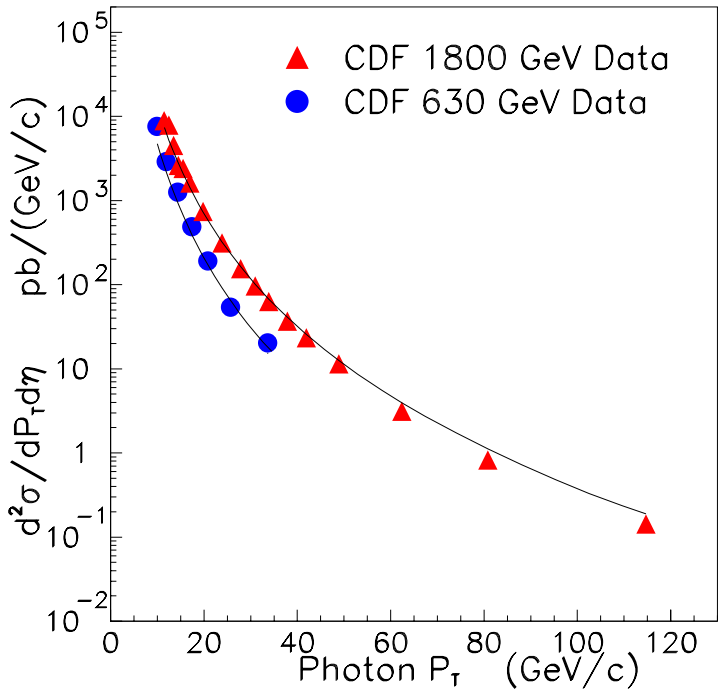

Figure 3: The inclusive photon cross sections at the two different center-of-mass energies compared to the next-to-leading order QCD predictions of ref. [13].

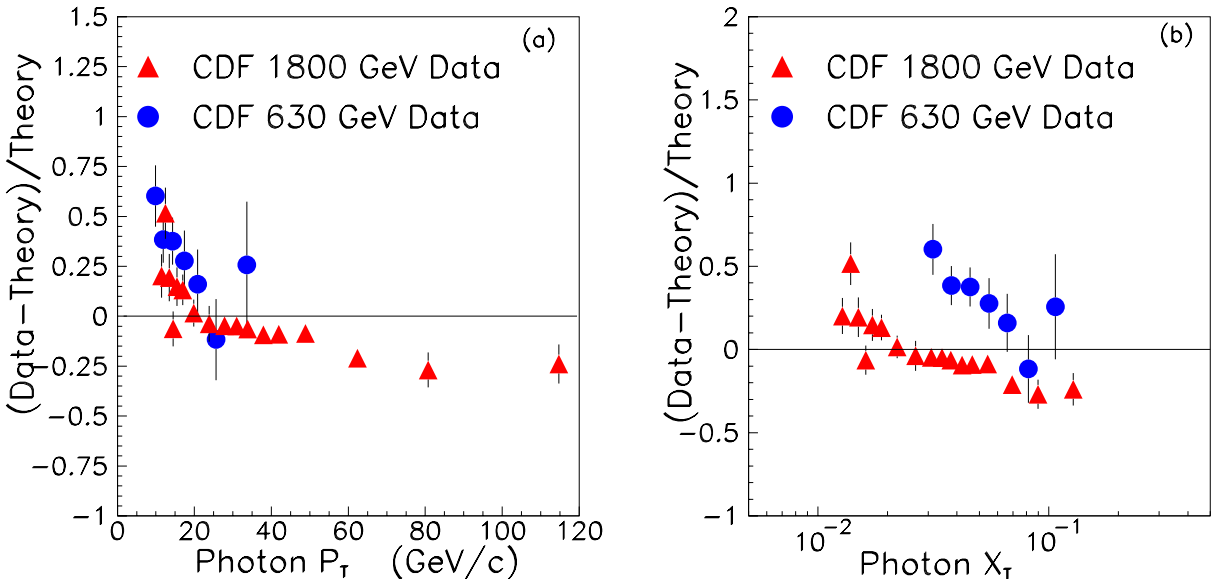

Figure 4: A comparison of the 1.8 TeV and 0.63 TeV data to a NLO QCD calculation [13] as a function of photon P_T and x_T. The NLO QCD calculation used the CTEQ5M parton distributions and a scale of $\mu = P_T$.

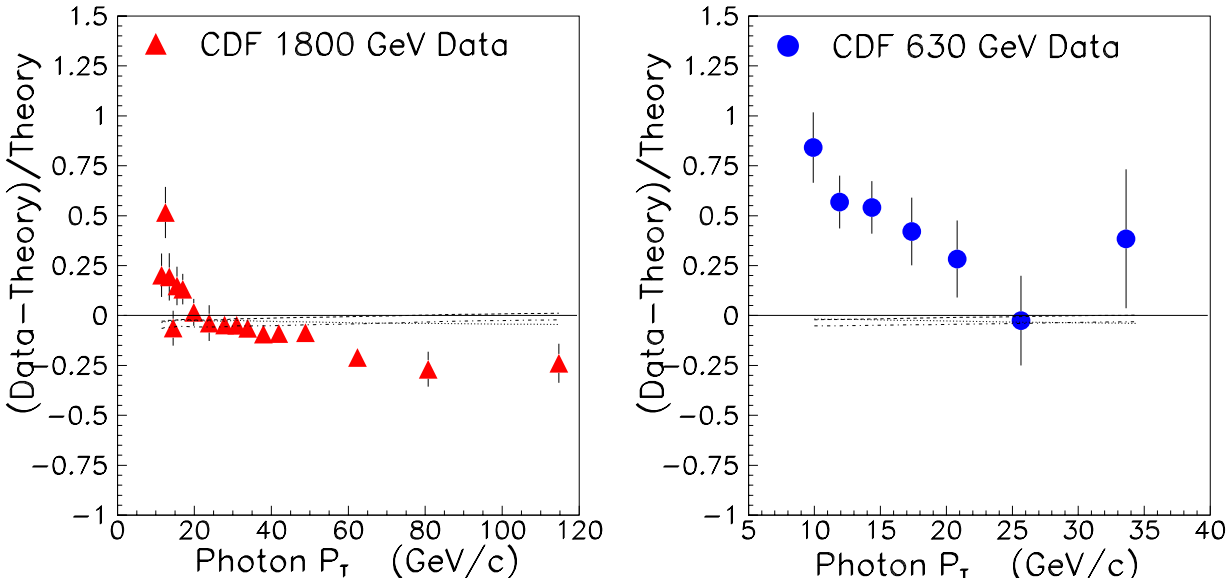

Figure 5: A comparison of the 1.8 TeV and 0.63 TeV differential cross sections to NLO QCD calculations using different parton distribution functions: CTEQ5M [14] (solid line), CTEQ5HJ [14] (dashed line), MRST-99 [16] (dotted line), MRST-99 $g \uparrow$ [16] (dot-dash line). All calculations use a scale of $\mu = P_T$.

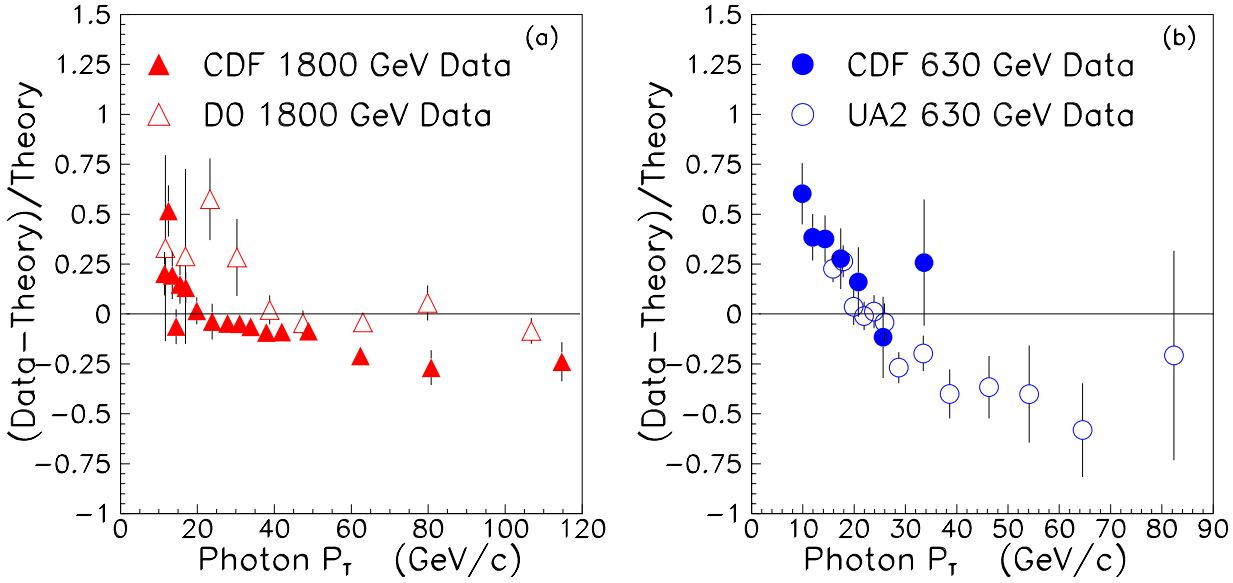

Figure 6: A comparison of the CDF and D0 1.8 TeV data sets and the CDF and UA2 630 GeV data sets to the same NLO QCD calculation [13] as Figure 4. There is excellent agreement between the CDF and UA2 data sets. The CDF and D0 data sets differ in normalization by about 20%, consistent with the quoted correlated systematic uncertainties of the measurements. The correlated systematic uncertainties for the D0 data are 10% at large P_T growing to 74% in the lowest P_T bin. CDF's correlated systematic uncertainties are listed in Tables 2 and 3, and are 11% at large P_T growing to 18% in the lowest P_T bin.

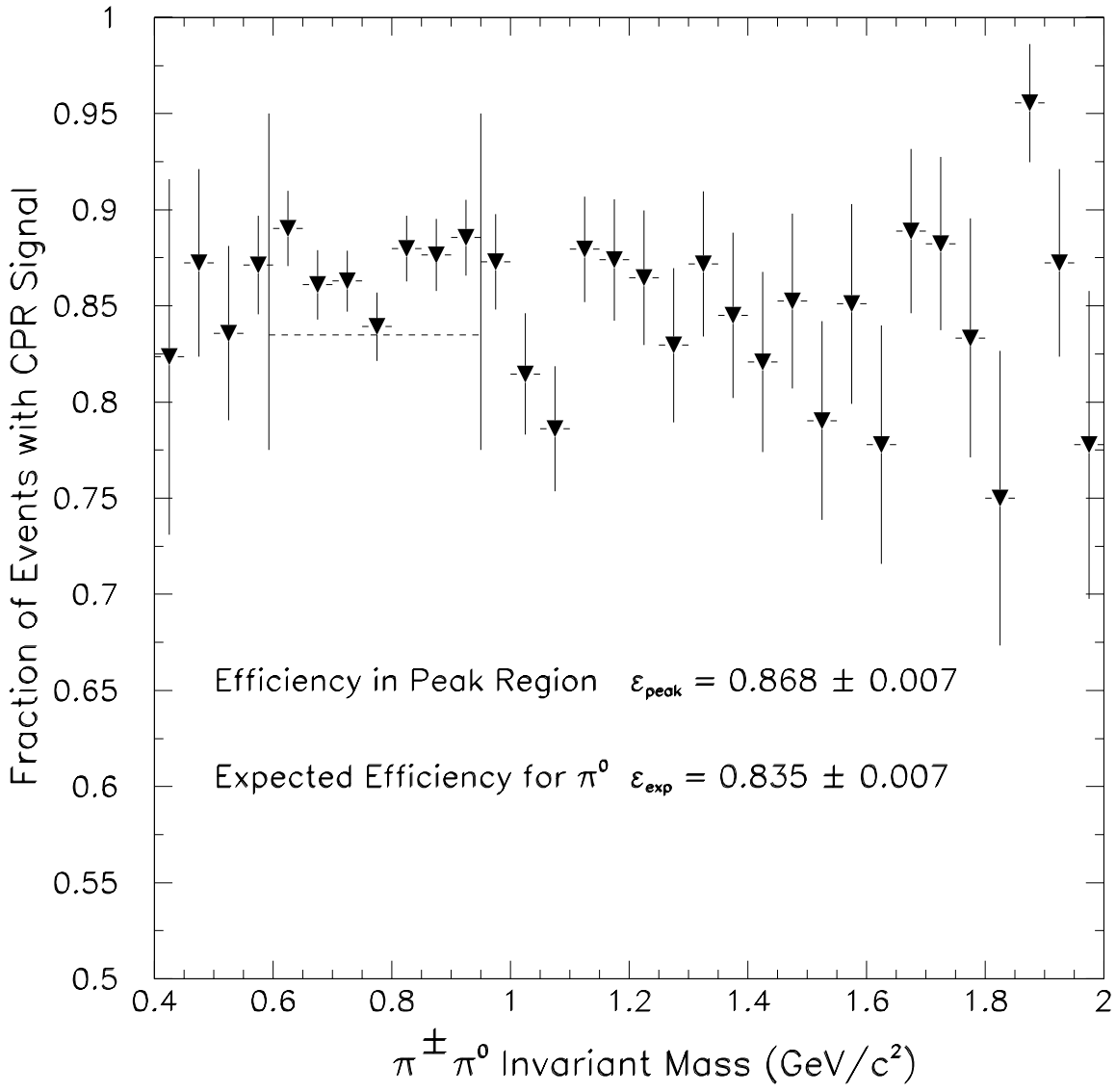

Figure 7: The fraction of events with a CPR signal is shown as a function of measured invariant mass in the $\rho^{\pm}$ sample. The dashed line shows the expected π^0 CPR signal rate in the ρ meson peak region.